

Effect of Nanoplatelet Size on the Colloidal Stability of Coupled Nanocomposite of TiO₂ and Zirconium Phosphate Nanoplatelets

Xiao YUAN¹, Songping MO^{1,2*}, Ying CHEN¹, Lin ZHENG¹, Lisi JIA¹, Tao YIN¹, Zhi YANG¹, Zhengdong CHENG^{1,2}

¹ Guangdong Provincial Key Laboratory on Functional Soft Condensed Matter, School of Materials and Energy, Guangdong University of Technology, Guangzhou 510006, China

² Artie McFerrin Department of Chemical Engineering, Texas A & M University, College Station, Texas 77843-3122, USA

crossref <http://dx.doi.org/10.5755/j01.ms.24.2.18154>

Received 10 May 2017; accepted 15 August 2017

The aggregation and sedimentation of nanoparticles affect the dispersion stability and application of nanosuspension. TiO₂ nanoparticles were coupled on zirconium phosphate (ZrP) disks with different diameters to study the effect of ZrP size on the dispersion stability of nanocomposite suspensions. Four suspensions, namely, TiO₂ nanosuspensions and three exfoliated TiO₂–ZrP nanocomposite suspensions with diameters of 729.6, 1004.5 and 1168.5 nm were prepared. Dispersion stability was compared among the suspensions. The zeta potential, viscosity, particle morphology and particle size distribution of the suspensions were also tested to analyze the stability mechanism of the nanocomposite suspensions. Results of the stability tests within 100 days show that the TiO₂–ZrP nanocomposite suspensions exhibited slower sedimentation, higher ultraviolet-visible absorbance, smaller light transmission and backscattering variation and lower Turbiscan Stability Index than those of the pure TiO₂ suspension. Among the samples, the smallest TiO₂–ZrP nanocomposites exhibited improved stability. The absolute zeta potential and viscosity of each nanocomposite suspension were comparable with one another, but higher than those of the TiO₂ suspension. The transmission electron microscope images and particle size distribution suggest that TiO₂–ZrP can better control the aggregation of small TiO₂ nanoparticle clusters.

Keywords: colloidal stability, nanocomposite, TiO₂, zirconium phosphate, size, aggregation.

1. INTRODUCTION

Extensive research on nanoparticles has been conducted in recent years as they have many potential applications. For example, TiO₂ nanoparticles have several advantages such as high chemical stability, high catalytic activity and nontoxicity; as such these particles exhibit potential for applications in photocatalysts [1, 2], solar cells [3], pollutant removal [4, 5] and cold thermal energy storage (TES) [6–11].

However, suspended nanoparticles tend to aggregate because of their high specific surface area and high surface energy, restricting their development for potential application. Thus, nanoparticles should be uniformly dispersed in the base fluids and maintained as stable in the suspensions. Most studies have focused on using surfactants and polymers as dispersants to stabilize nanoparticles against aggregation [12–20]. For TiO₂ nanoparticles, several types of surfactants have been used to improve the stability of nanosuspensions in previous studies, such as sodium dodecyl benzene sulfonate (SDBS) [21–23], sodium dodecyl sulfate (SDS) [24–26], cetyltrimethylammonium bromide (CTAB) [24, 27, 28] and polyvinylpyrrolidone (PVP) [29, 30]. The ionic surfactants, including SDBS, SDS and CTAB led to electrostatic repulsion between particles, which significantly reduced the particle agglomeration owing to van der Waals forces of attraction. Nonionic surfactants, such as PVP, caused a

hindrance between the particles, which can inhibit the nanoparticle aggregation to maintain good suspension stability.

Our preliminary experimental studies indicate that the size of TiO₂ nanoparticle aggregation would decrease through the hindrance effect caused by zirconium phosphate (ZrP) nanoplatelets without the use of surfactants [31]. We previously proposed a new method to improve TiO₂ suspension stability by coupling TiO₂ nanoparticles on ZrP nanoplatelets [32]. Particle size affects dispersion stability [33, 34]. However, the effect of nanoplatelet size on dispersion stability remains unknown and the mechanism for stability improvement is still unclear.

In this study, the dispersion stability of TiO₂–ZrP nanoplatelet suspensions with different diameters is investigated and compared with that of TiO₂ suspension. The effects of nanoplatelet size and dispersion mechanism of TiO₂–ZrP nanosuspensions were analyzed.

2. EXPERIMENTAL DETAILS

2.1. Synthesis of ZrP disks

The hydrothermal method was used to synthesize ZrP disks. Phosphoric acid (H₃PO₄, analytical reagent, Guangzhou Chemical Reagent Factory, China) and zirconium oxychloride octahydrate (ZrOCl₂·8H₂O, analytical reagent, Tianjin Fu Chen Chemical Reagent Factory, China) were the main reactants. ZrP disks of different diameters can be synthesized by controlling the

* Corresponding author. Tel: +862039322570; fax: +862039322570.
E-mail address: mosp@ustc.edu (S. Mo)

reaction duration time and temperature [35]. A sample of 10.0 g $\text{ZrOCl}_2 \cdot 8\text{H}_2\text{O}$ was mixed with 100 ml of H_3PO_4 sealed into the Teflon pressure vessel and heated at 200 °C for 10, 15 and 24 h to prepare ZrP of different sizes. After the reaction, the final products were identified as ZrP (10 h), ZrP (15 h) and ZrP (24 h) (Fig. 1). A scanning electron microscope (SEM, S3400N, Hitachi, Japan) was used to observe the shape and the approximate particle size of ZrP disks. The average diameters of the disks were different.

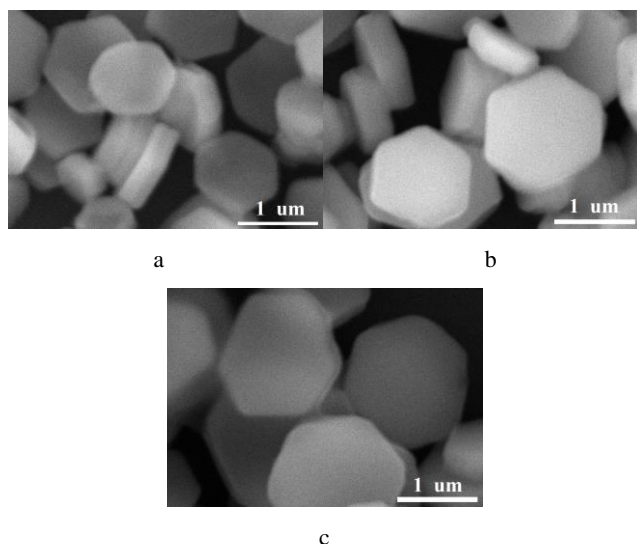


Fig. 1. SEM images: a–ZrP (10 h); b–ZrP (15 h); c–ZrP (24 h)

The size distribution (Fig. 2), average diameter and polydispersity (Table 1) of the exfoliated platelets were measured by using a dynamic light scattering (DLS) instrument (Delsa Nano C, Beckman Coulter Instruments Corporation, Fullerton, California) [36]. The results show that the ZrP disks have different sizes but similar size distributions and polydispersities. The small polydispersity and narrow size distribution indicated that these three kinds of ZrP disks have good uniformity [37].

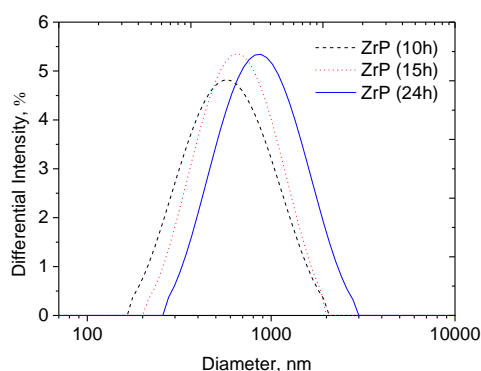


Fig. 2. Size distribution of ZrP nanodisks

Table 1. Size characterization of ZrP nanodisks

Sample	Average size	Polydispersity
ZrP (10 h)	729.6 nm	24.7 %
ZrP (15 h)	1004.5 nm	27 %
ZrP (24 h)	1168.5 nm	28.7 %

2.2. Coupling TiO_2 on ZrP disks

The ZrP loading TiO_2 (TiO_2 -ZrP) was synthesized using a three-step approach [19]. 3-(Triethoxysilyl) propyl isocyanate (IPTS, $\text{C}_{10}\text{H}_{21}\text{NO}_4\text{Si}$, AR, Alfa Aesar), a silane coupling agent, was used to combine TiO_2 and ZrP. Dimethyl sulfoxide (DMSO, $\text{C}_2\text{H}_6\text{OS}$, AR, Tianjin Damao Chemical Reagent Factory, China) was utilized as the solvent. The morphology of TiO_2 -ZrP was observed using a JEOL-2100 transmission electron microscope (TEM), as shown in Fig. 3 a, b and c. The average diameter of anatase TiO_2 (Alfa Aesar) was 32 nm, as illustrated in Fig. 3 d.

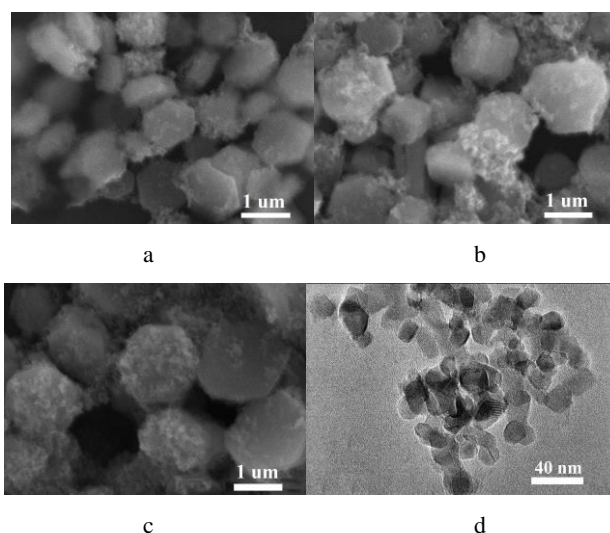


Fig. 3. The SEM images: a– TiO_2 -ZrP (729.6 nm); b– TiO_2 -ZrP (1004.5 nm); c– TiO_2 -ZrP (1168.5 nm); d–the TEM image of TiO_2

2.3. Preparation of TiO_2 -ZrP nanosuspensions

Two kinds of samples, namely, TiO_2 nanosuspension and exfoliated TiO_2 -ZrP nanosuspension, were prepared for the experiments. TiO_2 nanosuspension was prepared by adding 1 g of TiO_2 into 100 ml of deionized water. TiO_2 -ZrP suspension was prepared by adding 3 g TiO_2 -ZrP (mass ratio of 1:2) into 100 ml of DI water. TiO_2 -ZrP was then exfoliated into nanoplatelets in the suspensions. The mass ratio of the TiO_2 nanoparticles of all the samples was 1 wt.%, and the mass ratio of ZrP was 2 wt.%.

3. RESULTS AND DISCUSSION

3.1. Stability experiment

Fig. 4 shows the sedimentation image of samples and UV-vis absorption spectra after 100 days. The height of the suspension decreases in the sequence of TiO_2 -ZrP (729.6 nm), TiO_2 -ZrP (1004.5 nm), TiO_2 -ZrP (1168.5 nm) and TiO_2 , with the height of TiO_2 -ZrP (729.6 nm) remaining almost unchanged on the 100 th day. Ultraviolet-visible (UV-vis) absorption spectra (Fig. 4 b) were used to quantitatively evaluate the stability of the samples. The TiO_2 -ZrP suspension had higher absorbance compared with the TiO_2 suspension. The absorbance of TiO_2 -ZrP (729.6 nm) was approximately 6.67 % higher than that of the TiO_2 -ZrP (1004.5 nm) suspension, and the

absorbance of TiO₂-ZrP (1004.5 nm) was 25 % higher than that of the TiO₂-ZrP (1168.5 nm) suspension. The result shows that TiO₂-ZrP (729.6 nm) suspensions exhibited the optimal stability, and the decreasing sequence of suspensions is TiO₂-ZrP (729.6 nm), TiO₂-ZrP (1004.5 nm), TiO₂-ZrP (1168.5 nm) and TiO₂.

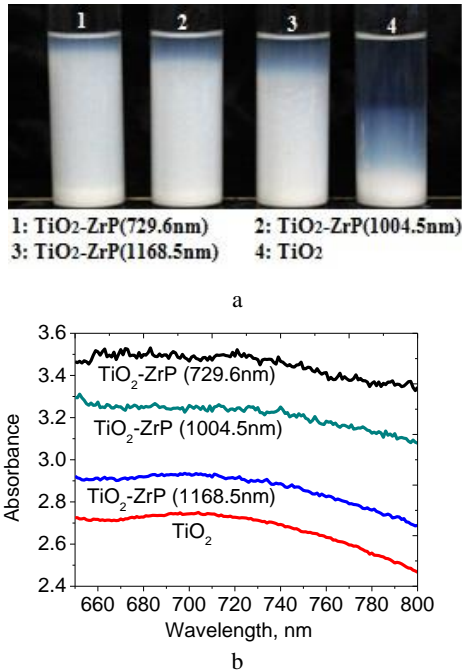


Fig. 4. a–sedimentation image of the samples; b–UV-vis absorption spectra

A novel optical analyzer, Turbiscan Lab (Formulation, France) equipment, which can measure the dispersion state through multiple light scattering data, was used to analyze the sedimentation phenomenon [38]. In the test, the particle suspensions were transferred to a glass cylindrical cell (70 mm height and 27.5 mm external diameter) and analyzed using a light beam, which periodically scanned the sample cell from the bottom to the top. The transmission (T) and backscattering (BS) optical sensors received the light that goes across the sample and scattered backward synchronously. When sedimentation took place, the T profiles varied with the cell height over time. Fig. 5 shows the T and BS profiles obtained from Turbiscan Lab, which indicate the light percentage transmitted through and scattered by the sample versus the sample cell height for TiO₂-ZrP and TiO₂ suspensions. The x and y axes in the T diagram represent the sample cell height and the variation of transmitted light and backscattering throughout the sample cell. Obviously, TiO₂ (Fig. 5 d) exhibited high transmission at about 42 mm sample cell height, which indicates that TiO₂ showed rapid aggregation. On the contrary, TiO₂-ZrP maintained moderate and low transmission, suggesting its higher stability than TiO₂.

A quantitative analysis was conducted using the Turbiscan Stability Index (TSI) to estimate the suspension

stability. This parameter is a statistical factor and its values are obtained as the sum of all processes taking place in the studied probe. The TSI values were calculated with the special computer program using the following equation [39]:

$$TSI = \sqrt{\frac{\sum_{i=1}^n (x_i - x_{BS})^2}{n-1}}, \quad (1)$$

where x_i is the mean backscattering for each minute of measurement, x_{BS} is the mean x_i , and n is the number of scans.

Fig. 6 shows the TSI values. Small TSI value represents better stability [39]. As the diameter of ZrP nanoplatelets decreased, the TSI value also decreased, indicating enhanced dispersion stability.

3.2. Zeta potential analysis

The possible reason for the stability difference is zeta potential. The relationship between suspension stability and zeta potential arises from the mutual repulsion that occurs between charged particles. For this reason, particles with high surface charge tend not to aggregate. Table 2 and Table 3 show the zeta potential values of the suspensions and the typically accepted corresponding relationship between zeta potential values and stability [40], respectively. As shown, the absolute zeta potential value of TiO₂ was in the unstable range (0, 15). The absolute zeta potential values of ZrP nanoplatelets (53.11 mV, 57.13 mV and 57.6 mV) were within the range (45, 60). After coupling TiO₂ on ZrP, the absolute zeta potential values of TiO₂-ZrP (49.12 mV, 50.14 mV and 55.9 mV) decreased slightly compared with ZrP but were still in the good stable range (45, 60). The results indicated that TiO₂-ZrP with a high surface charge is more difficult to aggregate and has better stability compared with TiO₂.

3.3. Aggregation size analysis

The viscosity and the aggregation size are important parameters that influence the particle sedimentation rate [41]. Fig. 7 shows the viscosity properties of the samples. The shear rate ranged from 1 s⁻¹ to 10³ s⁻¹. The viscosity curve of TiO₂-ZrP slowly declined along with the shear rate increase. The viscosity of TiO₂ was much lower than that of the TiO₂-ZrP suspensions. In general, the aggregation sedimentation rate decreased along with the suspension viscosity increase [41]. Thus, TiO₂-ZrP suspension has better stability than TiO₂. However, the viscosity is not enough to explain the results of sedimentation experiment because the viscosities of TiO₂-ZrP (729.6 nm), TiO₂-ZrP (1004.5 nm) and TiO₂-ZrP (1168.5 nm) are almost the same, but their stabilities are different. Thus, aggregation size is another important fact that can affect the stability of the suspensions.

Table 2. Zeta potential of TiO₂, TiO₂-ZrP and ZrP suspensions

Samples	TiO ₂	TiO ₂ -ZrP (729.6 nm)	TiO ₂ -ZrP (1004.5 nm)	TiO ₂ -ZrP (1168.5 nm)	ZrP (729.6 nm)	ZrP (1004.5 nm)	ZrP (1168.5 nm)
Z potential, mv	-14.92	-49.12	-50.14	-55.9	-53.11	-57.13	-57.6

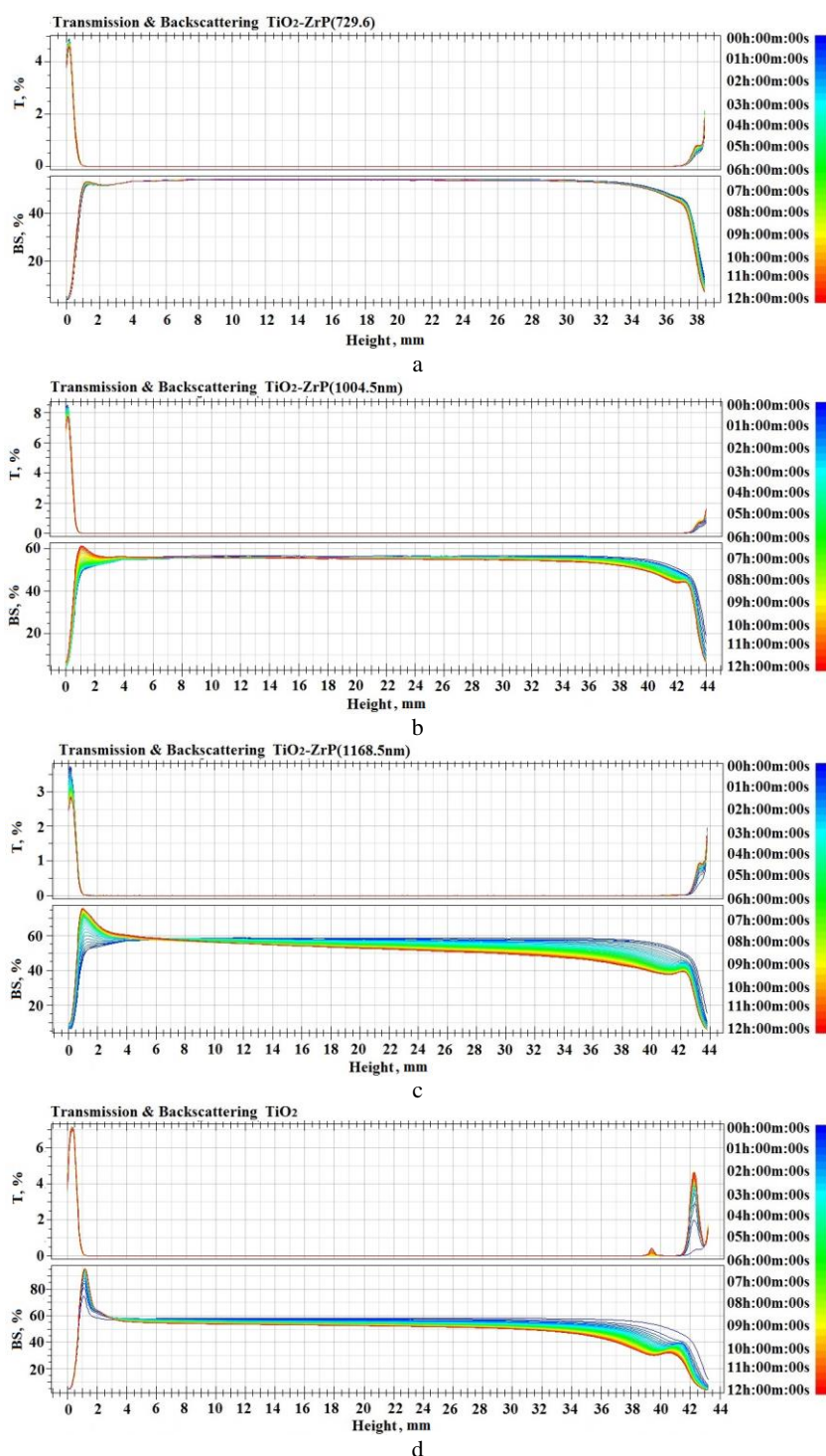


Fig. 5. T and BS versus sample height for: a – TiO₂–ZrP (729.6 nm); b – TiO₂–ZrP (1004.5 nm); c – TiO₂–ZrP (1168.5 nm); d – TiO₂

Table 3. Zeta potential and associated suspension stability

Z potential (absolute value, mv)	Stability
0	Little or no stability
15	Some stability but settling lightly
30	Moderate stability
45	Good stability, possible settling
60	Very good stability, little settling likely

The TEM images of TiO₂-ZrP and TiO₂ were recorded on the 100th day to get a better look at the aggregation of the samples. As shown in Fig. 8, TiO₂ became large

aggregations. In contrast, the TiO₂ aggregations distributed on the ZrP platelets was smaller because TiO₂ nanoparticles are fixed on the surface of the ZrP nanoplatelets, making them unable to aggregate into large particles.

Dynamic light scattering analysis is a common method used to measure the particle size distribution. Fig. 9 shows the particle size distribution of the TiO₂-ZrP and TiO₂ samples on the 0th and 100th day. The results show that aggregation appeared in TiO₂ and TiO₂-ZrP suspensions. Given that the primary size of the single TiO₂ particle is 30–60 nm, the particles in the pure TiO₂ suspension

aggregated considerably to about 10 nm on the 0th day. The TiO₂-ZrP aggregation size was evidently smaller compared with that of TiO₂ aggregation as TiO₂ loaded on the ZrP nanoplatelets.

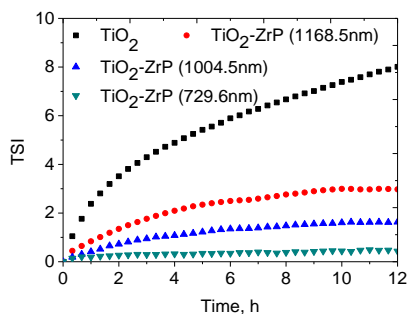


Fig. 6. TSI values of TiO₂ and TiO₂-ZrP suspensions

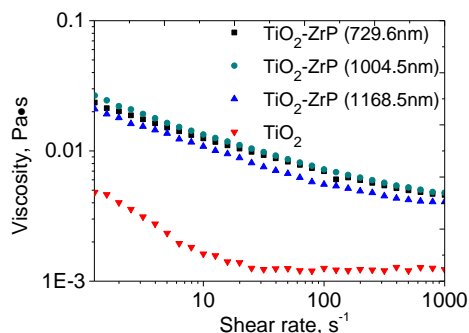


Fig. 7. Viscosity of TiO₂-ZrP and TiO₂

Table 4 shows that TiO₂ has more size distribution peaks and bigger aggregation size compared to TiO₂-ZrP on the 100th day. The aggregation sizes of TiO₂-ZrP (1168.5 nm), TiO₂-ZrP (1004.5 nm) and TiO₂-ZrP (729.6 nm) were 11368.5, 7240.1 and 5642.6 nm, respectively. The aggregation size decreased along with the diameter. Owing to the viscosity increment and aggregation size decrease, the sedimentation rate of TiO₂-ZrP slowed down compared with TiO₂. In addition, the sedimentation of smaller TiO₂-ZrP is even slower.

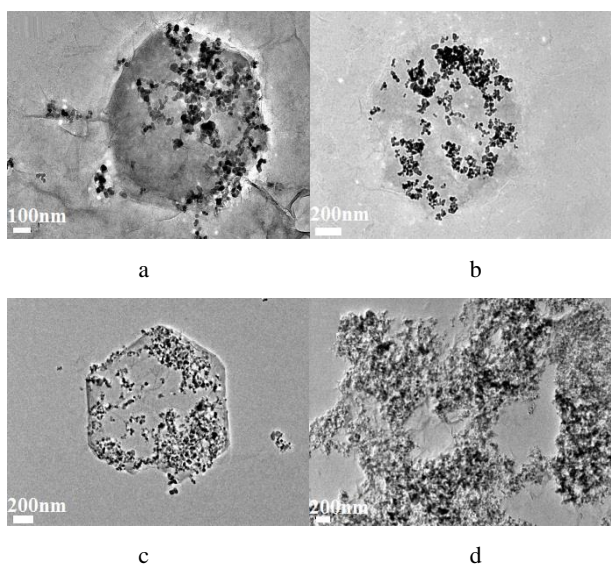


Fig. 8. TEM images: a-TiO₂-ZrP (729.6 nm); b-TiO₂-ZrP (1004.5 nm); c-TiO₂-ZrP (1168.5 nm); d-TiO₂

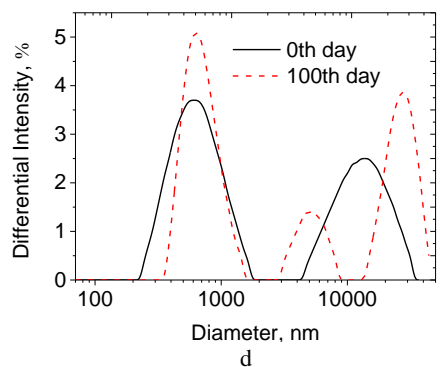
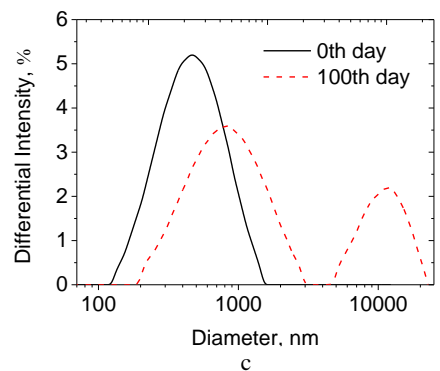
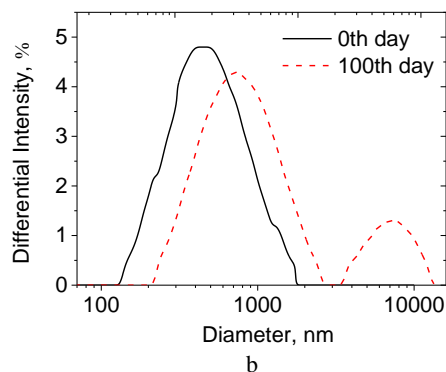
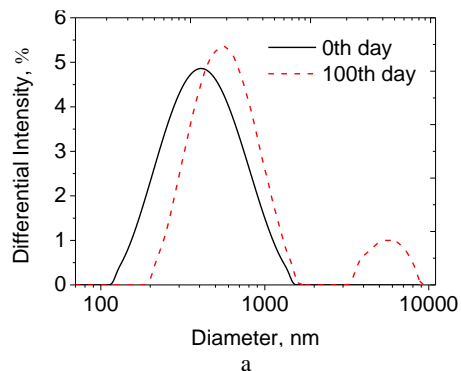


Fig. 9. Particles size distributions: a-TiO₂-ZrP (729.6 nm); b-TiO₂-ZrP (1004.5 nm); c-TiO₂-ZrP (1168.5 nm); d-TiO₂ on the 0th and 100th day

The experimental results of stability improvement achieved through coupling ZrP of different sizes can be explained by the effect of ZrP on controlling aggregation, and Brownian motion of particles. For the pure TiO₂ suspension, the zeta potential is low. Thus, the interparticle electrostatic repulsion cannot balance the van der Waals attraction, causing the particles to aggregate (Fig. 8 and Fig. 9) because they continually collide with each other owing to Brownian motion.

Table 4. Aggregation size of TiO₂-ZrP and TiO₂ on the 100th day

Sample	Average Size		Size distribution at 100 th day		
	0 th day	100 th day	Peak 1	Peak 2	Peak 3
TiO ₂ -ZrP (729.6 nm)	492.2 nm	543.3 nm	400.1 nm	5642.6 nm	–
TiO ₂ -ZrP (1004.5 nm)	541.8 nm	727.5 nm	586.5 nm	7240.1 nm	–
TiO ₂ -ZrP (1168.5 nm)	675 nm	1001.9 nm	533.6 nm	11368.5 nm	–
TiO ₂	1439.5 nm	1651 nm	717 nm	5233.1 nm	27254.7 nm

Consequently, the TiO₂ particle aggregations were large enough and settled down (Fig. 4) because gravity became significant. On the other hand, the well dispersion of particle aggregations may be maintained because of Brownian motion if they can be controlled to be small enough [34]. The ratio of gravitational to Brownian forces can be determined as follows

$$R_{Bg} = a^4 \Delta \rho g / (k_B T), \quad (2)$$

where a is the radius of particles, $\Delta \rho$ is the density difference between the particles and the base fluid, g is the gravitational acceleration, k_B is the Boltzmann constant and T is the temperature. The dispersion stability of suspension can be predicted using Eq. 2. If $R_{Bg} > 1$, particle (or aggregation) sedimentation can be expected, otherwise, the suspension is likely to be stable. Fig. 10 shows the plot of R_{Bg} determined based on Eq. 2.

If the aggregation size is larger than 1430 nm, which is the case of pure TiO₂ suspension even at the first day (Table 4), then $R_{Bg} > 1$ and the aggregation will settle down because of gravity, as shown in Fig. 4. As for TiO₂-ZrP nanoplatelets, TiO₂ nanoparticles were fixed with ZrP, and the surface charge prevented the nanoplatelets to aggregate. The TiO₂-ZrP suspension stability were much better than that of TiO₂ suspension because the sizes of the three types of TiO₂-ZrP nanoplatelet were all smaller than 1002 nm even at day 100 (Table 4).

Moreover, smaller ZrP resulted to smaller particle aggregation of TiO₂-ZrP, thus indicating better dispersion stability (Fig. 10). There are two reasons, one is that the TiO₂ nanoparticles are fixed on ZrP and their aggregation is better controlled by smaller ZrP nanoplatelets, and the other is attributed to the steric stabilization effect of the ZrP nanoplatelets [31]. The number concentration of the smaller ZrP nanoplatelets is higher than that of larger ZrP nanoplatelets at the same ZrP mass concentration. Therefore, the smaller ZrP nanoplatelets better separated the particle aggregates and better control further aggregation at the same ZrP mass concentration.

4. CONCLUSIONS

In this study TiO₂ nanoparticles were coupled on ZrP platelets with different diameters to study the effect of platelet size on the colloidal stability of suspensions of the coupled nanocomposite. Main conclusions were obtained as follows:

1. By coupling TiO₂ on ZrP nanoplatelets with diameters of 729.6 nm, 1004.5 nm and 1168.5 nm, the TiO₂ suspensions' absolute value of zeta potential can be increased, their sedimentation can decrease, and their dispersion stability can be improved.

2. The dispersion stability of TiO₂-ZrP suspensions increased along with the decreased in ZrP diameter because their aggregation is better controlled by smaller ZrP nanoplatelets. The first reason is that the TiO₂ nanoparticles are fixed on smaller ZrP nanoplatelets and the other reason is that there are more ZrP nanoplatelets for smaller ZrP nanoplatelets at the same ZrP mass concentration to separate the TiO₂ nanoparticles.

Acknowledgments

The authors acknowledge the financial support provided by the Natural Science Foundation of China (NSFC) under contract No. 51576050, the Project of Guangdong Provincial Science and Technology Plan (No. 2015A010106013) and the Science and Technology Program of Guangzhou (No. 201704030107). S. Mo acknowledges the support of the State Scholarship Funded by the China Scholarship Council.

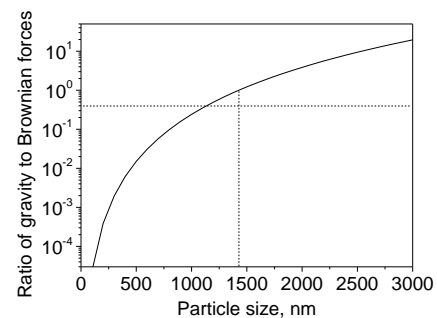


Fig. 10. Ratio of gravitational to Brownian forces versus particle size

REFERENCES

1. **Chen, L.J., Tian, J.T., Qiu, H., Yin, Y.S., Wang, X., Dai, J.H., Wu, P.W., Wang, A.P., Chu, L.** Preparation of TiO₂ Nanofilm via Sol-gel Process and its Photocatalytic Activity for Degradation of Methyl Orange *Ceramic International* 35 2009: pp. 3275–3280. <https://doi.org/10.1016/j.ceramint.2009.05.021>
2. **Fujishima, A., Zhang, X.T., Tryk, D.A.** TiO₂ Photocatalysis and Related Surface Phenomena *Surface Science Reports* 63 2008: pp. 515–582. <https://doi.org/10.1016/j.surfrep.2008.10.001>
3. **An'amt, M.N., Radiman, S., Huang, N.M., Yarmo, M.A., Ariyanto, N.P., Lim, H.N., Muhamad, M.R.** Sol-gel Hydrothermal Synthesis of Bismuth-TiO₂ Nanotubes for Dye-sensitized Solar Cell *Ceramics International* 36 2010: pp. 2215–2220. <https://doi.org/10.1016/j.ceramint.2010.05.027>
4. **Altın, İ., Sökmen, M., Bıyıkhoğlu, Z.** Sol Gel Synthesis of

- Cobalt Doped TiO₂ and its Dye Sensitization for Efficient Pollutant Removal *Materials Science in Semiconductor Processing* 45 2016: pp. 36–44.
<https://doi.org/10.1016/j.mssp.2016.01.016>
5. **Lalhriatpuia, C., Tiwari, D., Tiwari, A., Lee, S.M.** Nanopillars-TiO₂ in the Efficient Removal of Micro-Pollutants from Aqueous Solutions: Physico-chemical Studies *Chemical Engineering Journal* 281 2015: pp. 782–792.
<https://doi.org/10.1016/j.cej.2015.07.032>
 6. **Mo, S.P., Chen, Y., Jia, L.S., Luo, X.L.** Investigation on Crystallization of TiO₂-water Nanofluids and Deionized Water *Applied Energy* 93 2012: pp. 65–70.
<https://doi.org/10.1016/j.apenergy.2011.07.014>
 7. **Mo, S.P., Chen, Y., Jia, L.S., Luo, X.L.** Reduction of Supercooling of Water by TiO₂ Nanoparticles as Observed Using Differential Scanning Calorimeter *Journal of Experimental Nanoscience* 8 2013: pp. 533–539.
<https://doi.org/10.1080/17458080.2011.572085>
 8. **Li, X., Chen, Y., Cheng, Z.D., Jia, L.S., Mo, S.P., Liu, Z.W.** Ultrahigh Specific Surface Area of Graphene for Eliminating Subcooling of Water *Applied Energy* 130 2014: pp. 824–829.
<https://doi.org/10.1016/j.apenergy.2014.02.032>
 9. **Mo, S.P., Chen, Y., Cheng, Z.D., Jia, L.S., Luo, X.L., Shao, X.F., Yuan, X., Lin, G.** Effects of Nanoparticles and Sample Containers on Crystallization Supercooling Degree of Nanofluids *Thermochimica Acta* 605 2015: pp. 1–7.
<https://doi.org/10.1016/j.tca.2015.02.006>
 10. **Jia, L.S., Chen, Y., Mo, S.P.** Solid-liquid Phase Transition of Nanofluids *International Journal of Heat & Mass Transfer* 59 (1) 2013: pp. 29–34.
<https://doi.org/10.1016/j.ijheatmasstransfer.2012.11.044>
 11. **Jia, L.S., Peng, L., Chen, Y., Mo, S.P., Li, X.** Improving the Supercooling Degree of Titanium Dioxide Nanofluids with Sodium Dodecylsulfate *Applied Energy* 124 (7) 2014: pp. 248–255.
 12. **Farrokhpay, S.** A Review of Polymeric Dispersant Stabilisation of Titania Pigment Saeed Farrokhpay *Advances in Colloid & Interface Science* 151 (1–2) 2009: pp. 24–32.
 13. **Wiącek, A.E., Anitowska, E., Delgado, A.V., Holysz, L., Chibowski, E.** The Electrokinetic and Rheological Behavior of Phosphatidylcholine-treated TiO₂ Suspensions *Colloids and Surfaces A: Physicochemical and Engineering Aspects* 440 (2) 2014: pp. 110–115.
<https://doi.org/10.1016/j.colsurfa.2012.09.054>
 14. **Karakaş, F., Çelik, M.S.** Mechanism of TiO₂ Stabilization by Low Molecular Weight NaPAA in Reference to Water-borne Paint Suspensions *Colloids and Surfaces A: Physicochemical and Engineering Aspects* 434 (19) 2013: pp. 185–193.
<https://doi.org/10.1016/j.colsurfa.2013.05.051>
 15. **Holmberg, J.P., Ahlberg, E., Bergenholtz, J., Hassellöv, M., Abbas, Z.** Surface Charge and Interfacial Potential of Titanium Dioxide Nanoparticles: Experimental and Theoretical Investigations *Journal of Colloid & Interface Science* 407 (10) 2013: pp. 168–176.
<https://doi.org/10.1016/j.jcis.2013.06.015>
 16. **Liu, Y., Yu, Z., Zhou, S., Wu, L.** De-agglomeration and Dispersion of Nano-TiO₂ in an Agitator Bead Mill *Journal of Dispersion Science & Technology* 27 (7) 2006: pp. 983-990.
 17. **Veronovski, N., Andreozzi, P., Mesa, C.L., Sfiligoj-Smole, M., Ribitsch, V.** Use of Gemini Surfactants to Stabilize TiO₂ P25 Colloidal Dispersions *Colloid & Polymer Science* 288 (288) 2010: pp. 387–394.
 18. **Imae, T., Muto, K., Ikeda, S.** The pH Dependence of Dispersion of TiO₂ Particles in Aqueous Surfactant Solutions *Colloid & Polymer Science* 269 (1) 1991: pp. 43–48.
 19. **Veronovski, N., Andreozzi, P., Mesa, C.L., Sfiligoj-Smole, M.** Stable TiO₂ Dispersions for Nanocoating Preparation *Surface & Coatings Technology* 204 (9–10) 2010: pp. 1445–1451.
 20. **Liu, W., Sun, W., Borthwick, A.G.L., Nia, J.** Comparison on Aggregation and Sedimentation of Titanium Dioxide, Titanate Nanotubes and Titanate Nanotubes-TiO₂: Influence of pH, Ionic Strength and Natural Organic Matter *Colloids and Surfaces A: Physicochemical and Engineering Aspects* 434 (19) 2013: pp. 319–328.
<https://doi.org/10.1016/j.colsurfa.2013.05.010>
 21. **Huang, J., Wang, X., Long, Q., Wen, X., Zhou, Y., Li, L.** Influence of pH on the Stability Characteristics of Nanofluids *In: Symposium on Photonics and Optoelectronics* 2009: pp. 1–4.
<https://doi.org/10.1109/SOPO.2009.5230102>
 22. **He, Q., Wang, S., Zeng, S., Zheng, Z.** Experimental Investigation on Photothermal Properties of Nanofluids for Direct Absorption Solar Thermal Energy Systems *Energy Conversion & Management* 73 (5) 2013: pp. 150–157.
<https://doi.org/10.1016/j.enconman.2013.04.019>
 23. **Meibodi, M.E., Vafaie-Sefti, M., Rashidi, A.M., Amrollahi, A., Tabasi, M., Kalal, H.S.** The Role of Different Parameters on the Stability and Thermal Conductivity of Carbon Nanotube/water Nanofluids *International Communications in Heat and Mass Transfer* 37 2010: pp. 319–23.
<https://doi.org/10.1016/j.icheatmasstransfer.2009.10.004>
 24. **Assael, M.J., Metaxa, I.N., Arvanitidis, J., Christofilos, D., Lioutas, C.** Thermal Conductivity Enhancement in Aqueous Suspensions of Carbon Multi-walled and Double-walled Nanotubes in the Presence of Two Different Dispersants *International Journal of Thermophysics* 26 2005: pp. 647–664.
<https://doi.org/10.1007/s10765-005-5569-3>
 25. **Ghadimi, A., Metselaar, I.H.** The Influence of Surfactant and Ultrasonic Processing on Improvement of Stability, Thermal Conductivity and Viscosity of Titania Nanofluid *Experimental Thermal and Fluid Science* 51 2013: pp. 1–9.
<https://doi.org/10.1016/j.expthermflusci.2013.06.001>
 26. **Nasiri, A., Shariaty-Niasar, M., Rashidi, A., Amrollahi, A., Khodafarin, R.** Effect of Dispersion Method on Thermal Conductivity and Stability of Nanofluid *Experimental Thermal and Fluid Science* 35 2011: pp. 717–723.
<https://doi.org/10.1016/j.expthermflusci.2011.01.006>
 27. **Chaji, H., Ajabshirchi, Y., Esmaeilzadeh, E., Heris, S.Z., Hedayatzadeh, M., Kahani, M.** Experimental Study on Thermal Efficiency of Flat Plate Solar Collector Using TiO₂/water Nanofluid *Modern Applied Science* 7 (10) 2013: pp. 60–69.
<https://doi.org/10.5539/mas.v7n10p60>
 28. **Lee, S.H., Jang, S.P.** Extinction Coefficient of Aqueous Nanofluids Containing Multiwalled Carbon Nanotubes *International Journal of Heat and Mass Transfer* 67 2013: pp. 930–935.
<https://doi.org/10.1016/j.ijheatmasstransfer.2013.08.094>

29. Prasad, G., Srinu, N.S., Komel, A., Srinath, S., Anand, K., Pydi, S.Y., Shirish, S. Stable Colloidal Copper Nanoparticles for a Nanofluid: Production and Application *Colloids & Surfaces A Physicochemical & Engineering A* 441 2014: pp. 589–597.
<https://doi.org/10.1016/j.colsurfa.2013.10.026>
30. Liu, T., Chen, W., Liu, X., Zhu, J., Lu, L. Well-dispersed Ultrafine Nitrogen-doped TiO₂ with Polyvinylpyrrolidone (PVP) Acted as N-source and Stabilizer for Water Splitting *Journal of Energy Chemistry* 25 (1) 2016: pp. 1–9.
<https://doi.org/10.1016/j.jechem.2015.11.009>
31. Liu, Z.W., Chen, Y., Cheng, Z.D., Mo, S.P., Li, H.W. Stability of TiO₂ Nanoparticles in Deionized Water with ZrP Nanoplatelets *Journal of Nanoscience and Nanotechnology* 15 (4) 2015: pp. 3271–3275.
<https://doi.org/10.1166/jnn.2015.9685>
32. Liu, Z., Yin, T., Chen, Y., Cheng, Z., Mo, S., Jia, L. Improving the Stability of TiO₂ Aqueous Suspensions by Coupling TiO₂ Nanoparticles on ZrP Nanoplatelets *Energy Procedia* 75 2015: pp. 2199–2204.
<https://doi.org/10.1016/j.egypro.2015.07.377>
33. Wiese, G.R., Healy, T.W. Effect of Particle Size on Colloid Stability *Transactions of the Faraday Society* 66 1970: pp. 490–499.
34. Larsson, M., Hill, A., Duffy, J. Suspension Stability: Why Particle Size, Zeta Potential and Rheology are Important *Malvern Instruments Limited* 20 2012: pp. 209–214.
35. Sun, L., Boo, W.J., Sue, H., Clearfield, A. Preparation of α -zirconium Phosphate Nanoplatelets with Wide Variations in Aspect Ratios *New Journal of Chemistry* 31 (1) 2007: pp. 39–43.
<https://doi.org/10.1039/B604054C>
36. Mejia, A.F., Chang, Y.W., Ng, R., Shuai, M., Mannan, M.S., Cheng, Z. Aspect Ratio and Polydispersity Dependence of Isotropic-nematic Transition in Discotic Suspensions *Physical Review E* 85 (6) 2012: pp. 061708.
<https://doi.org/10.1103/PhysRevE.85.061708>
37. Germain, V., Pileni, M.P. Size Distribution of Cobalt Nanocrystals: A Key Parameter in Formation of Columns and Labyrinths in Mesoscopic Structures *Advanced Materials* 17 (11) 2005: pp. 1424–1429.
<https://doi.org/10.1002/adma.200401559>
38. Fang, F.F., Liu, Y.D., Choi, H.J. Carbon Nanotube Coated Magnetic Carbonyl Iron Microspheres Prepared by Solvent Casting Method and Their Magneto-responsive Characteristics *Colloids & Surfaces* 412 (20) 2012: pp. 47–56.
<https://doi.org/10.1016/j.colsurfa.2012.07.013>
39. Wiśniewska, M. Influences of Polyacrylic Acid Adsorption and Temperature on the Alumina Suspension Stability *Powder Technology* 198 (198) 2010: pp. 258–266.
<https://doi.org/10.1016/j.powtec.2009.11.016>
40. Lee, J.H., Hwang, K.S., Jang, S.P., Lee, B.H., Kim, J.H., Choi, S.U.S., Choi, C.J. Effective Viscosities and Thermal Conductivities of Aqueous Nanofluids Containing Low Volume Concentrations of Al₂O₃ *International Journal of Heat and Mass Transfer* 51 (11–12) 2008: pp. 2651–2656.
<https://doi.org/10.1016/j.ijheatmasstransfer.2007.10.026>
41. Witharana, S., Palabiyik, I., Musina, Z., Ding, Y. Stability of Glycol Nanofluids—the Theory and Experiment *Powder Technology* 239 (17) 2013: pp. 72–77.
<https://doi.org/10.1016/j.powtec.2013.01.039>